

ABRASIVE FLOW MACHINING OF ADDITIVELY MANUFACTURED TITANIUM: THIN WALLS AND INTERNAL CHANNELS

S. S. Jalui¹, T. J. Spurgeon¹, E. R. Jacobs¹, A. Chatterjee², T. Stecko³, and G. P. Manogharan^{1*}

¹ Department of Mechanical Engineering, The Pennsylvania State University, University Park, PA 16801

² Department of Engineering Science and Mechanics, The Pennsylvania State University, University Park, PA 16801

³ The Center for Quantitative Imaging, The Pennsylvania State University, University Park, PA 16801

*Corresponding Author: gum53@psu.edu

Abstract

Metal additive manufacturing using Laser-Powder Bed Fusion (L-PBF) technique has enabled the metal manufacturing industry to use design tools with increased flexibility such as freeform internal channel geometries that benefit thermofluidic applications such as heat exchangers. A primary drawback of the L-PBF process is the as-built surface roughness, which is a critical factor in such surface-fluidic applications. In addition, complex internal channel geometries cannot be post-processed through traditional finishing and polishing methods, and require advanced finishing processes such as Abrasive Flow Machining (AFM). In this original study, the effects of AM design including geometrical changes at the inlets, internal channel and wall thickness of thin features are experimentally studied on Ti64 L-PBF parts. A novel surface roughness inspection technique using micro-CT data is also presented. The internal channels with larger dimensions underwent 40% improvement in surface roughness with no statistically significant change in diameter whereas the channels with smaller dimensions and bends had a 38% improvement in surface roughness accompanied by a 6% increase in diameter. While there was as much as 30% improvement in surface roughness values, the thin walls less than 0.4 mm in dimension were deformed under the AFM pressure after just 5 cycles.

Keywords: Laser-Powder Bed Fusion, Additive Manufacturing, Surface Roughness, Abrasive Flow Machining, Micro-CT Scanning, Hybrid AM

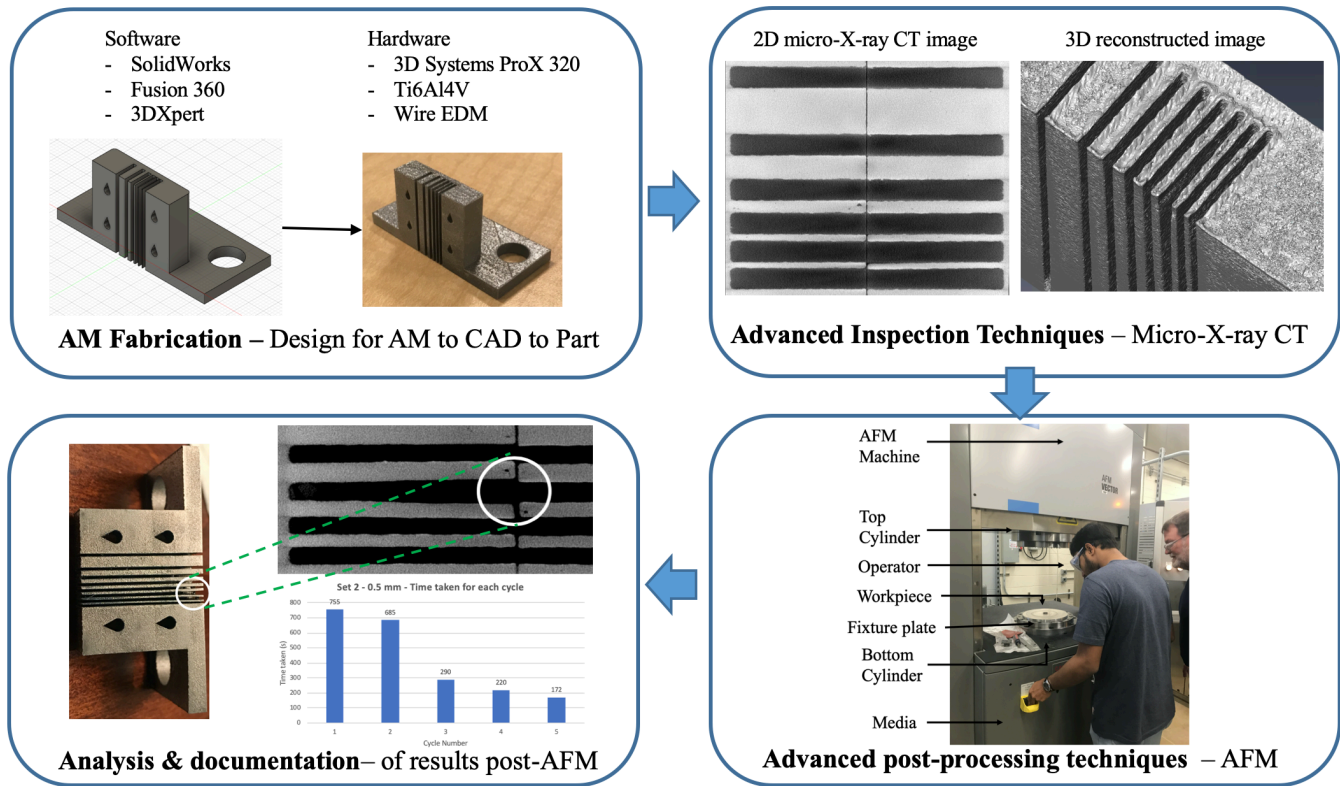


Figure 1: Graphical abstract

1. Introduction

Metal additive manufacturing has enabled the fabrication of complex geometries that could not be produced using conventional techniques. Several industries including aerospace, defense, and heavy machinery benefit by leveraging this in applications such as heat exchangers, heat sinks, fuel passages, and conformal cooling channels. Organic, free-form designs allow for these components to contain superior functionalities when compared to their conventional counterparts due advantages such as partlight-weighting, and optimized topologies. The global metal heat exchanger market was valued at \$15.3 billion in 2019 and estimated to grow to \$20.5 billion by 2024 [1]. Additionally, the injection molding industry currently stands at an impressive \$60 billion in the United States alone [2]. As per the AM Power report 2020, the aerospace, turbines, and helicopter industries accounted for 29% of all AM system sales revenue [3].

However, one of the biggest drawbacks of the metal Laser-based Powder Bed Fusion (L-PBF) AM process is the as-built surface roughness which typically ranges from 5-20 microns (Ra)[4][5][6][7]. Surface roughness is a critical factor for applications that include inaccessible features commonly found in gas turbines, heat exchangers, and injection molding conformal cooling channels. It impacts factors such as heat transfer, flow rate, boundary layer velocity, and ultimately efficiency of these components and their respective designs. Several finishing and polishing techniques have emerged such as milling, turning, abrasive jet machining, electro-chemical polishing, vibratory finishing, and abrasive flow machining, among others, that enable achieving the desired surface roughness values to ensure optimal performance. However, several challenges exist with using these processes on additively manufactured parts and their respective design intricacies. The critical surfaces within such internal passageways can be extremely hard

to reach by the tooling that is required in some of these finishing and polishing methods. Abrasive flow machining (AFM) is one such method that involves a visco-elastic polymer loaded with abrasives to enter and flow through complex internal passageways. Petare and Jain (2018) list the different variants of the AFM process that have emerged over the years [8]. Recent studies have shown the effects of traditional AFM on both conventionally [9][10][11] and additively manufactured surfaces. Bouland et. al (2019) proposed a model to predict material removal and surface roughness and found that there is a “river-bank” effect created at flat edges as a result of the AFM process [12]. Han et. al. (2020) performed AFM on additively manufactured through holes [13] and helical passageways [14] and reported an improvement in the areal roughness (S_a) values after 10 cycles. Duval-Chaneac et. al. (2018) performed multiple AFM cycles on SLM manufactured coupons using 4 different media with varying viscosity and analyzed the roughness evolution behavior along with residual stress analysis [15]. Kum et. al (2020) proposed a model to predict material removal caused by AFM on external AM surfaces using a combination of CFD and Neural Networks [16]. Fabrication of detailed features with small dimensions such as thin walls are subjected to large machining forces, capable of causing permanent deformations that may be critical to the application and structural integrity of the component. Deformation of thin walls and changes in dimensions coupled with defects such as keyhole porosity within the L-PBF process, could largely vary the actual performance of heat exchangers and gas turbine components from simulated results.

Another potential problem that arises in the context of AM parts is the method of inspection. In order to ensure non-destructively measured dimensions and surface roughness values of organically shaped surfaces, micro-CT scans serve as a viable option. However certain limitations such as specimen size and voxel approximation persists while using this process. Several studies show the use the micro-CT data for roughness measurements of additively manufactured samples. Snyder et al.[17] talks about the capabilities of CT scan software, and their abilities to detect and evaluate resolutions up to $1/10^{\text{th}}$ of the scans’ respective voxel size. Moreover, data from scans of $35\ \mu\text{m}$ voxel sizes resulted in a decrease in resolution via smoothing out some of the smaller features.

Townsend et al. [18] discussed the factors impacting the accuracy of areal surface data obtained using micro-CT for roughness measurements. They also established how internal and external surface data has the ability to impact edge boundary approximations and variations for similar surface textures. This, in turn, affected the roughness measurements using CT. Kerckhofs et al. [19] and Pyka et al. [20] investigated the use of micro-CT data to evaluate linear mean profile roughness using 2D slices of the surfaces under consideration. No statistical difference was found for surfaces having roughness values between $5\text{-}30\ \mu\text{m}$, in the means of P_a (an unfiltered raw profile’s average roughness) values derived using contact profilometry and micro-CT data. However, surfaces that contained sub-micron roughness values also had CT data that considerably overvalued the P_a values when compared to those obtained using a contact profilometry method, even with a $1.5\ \mu\text{m}$ voxel size.

Carmignato et al.[21] investigated the effects of surface roughness on dimensional measurements obtained using CT data. The findings included lower roughness values calculated using micro-CT when compared to experimentally obtained values, caused due to voxel approximation of peaks and valleys. It was also reported that the standard deviations of such data increased across the board with an increase in voxel size, resulting from effects being more pronounced for larger voxel values.

This paper focuses on studying the effects of the AFM process on the dimensions and roughness of additively manufactured titanium alloy specimens. The primary geometries under consideration were thin walls and internal channels with bends.

2. CAD design

The specimens were designed using Autodesk Fusion 360. Since the AFM process required fixturing, it was decided that the specimens will have a rectangular flange incorporated into the design to match the machining characteristics on our AFM machine. This ensured that the specimens could be swapped out easily. Additionally, the specimens were designed as two halves that would ensure that they could be taken apart between AFM cycles to help with visual inspection and facilitate the cleaning process to remove any remaining media. A footprint of 50 mm x 45 mm was chosen for the rectangular flange. An area of 26 mm x 14 mm around the center was chosen for the housing of the channels. Four 9 mm diameter bolt holes were created on the corners of the rectangular flange. To bolt the two halves of the specimens, bolt holes for standard bolts with 5 mm diameter heads and 1 mm diameter threads were created. In order to make these self-supporting, they were designed in teardrop shapes with 55 degree angles. A 12 mm x 10 mm rectangle housed the actual geometry of the channels that varied across samples. The specimen designs were separated into three sets with each representing different features under consideration. Set 1 consisted of a 10 mm diameter through hole. Set 2 consisted of rectangular slots with 1 mm, 0.5 mm, 0.25 mm, and 0.1 mm slot widths. Set 3 consisted of 4 mm diameter cylindrical channels with zero (through hole), one, and three bends. Each of the slots were separated by varying wall thicknesses as described in Table 1. To ensure that all surfaces were self-supporting, all bent, internal channel surfaces were at a 55 degree angle making the bend angle 110 degrees. A depiction of the cross-sections of all test specimen are shown in Figure 2.

Table 1: Wall thicknesses for Set 2 specimens

Channel Width (in mm)	Wall Thicknesses (in mm)
1	2, 1, 0.5, 0.25, 0.2
0.5	2, 1, 0.75, 0.6, 0.5, 0.4, 0.3
0.25	2, 1.5, 1, 0.75, 0.5, 0.4, 0.3, 0.25, 0.2, 0.1
0.1	2, 1.5, 1.25, 1, 0.75, 0.6, 0.5, 0.4, 0.3, 0.2, 0.1

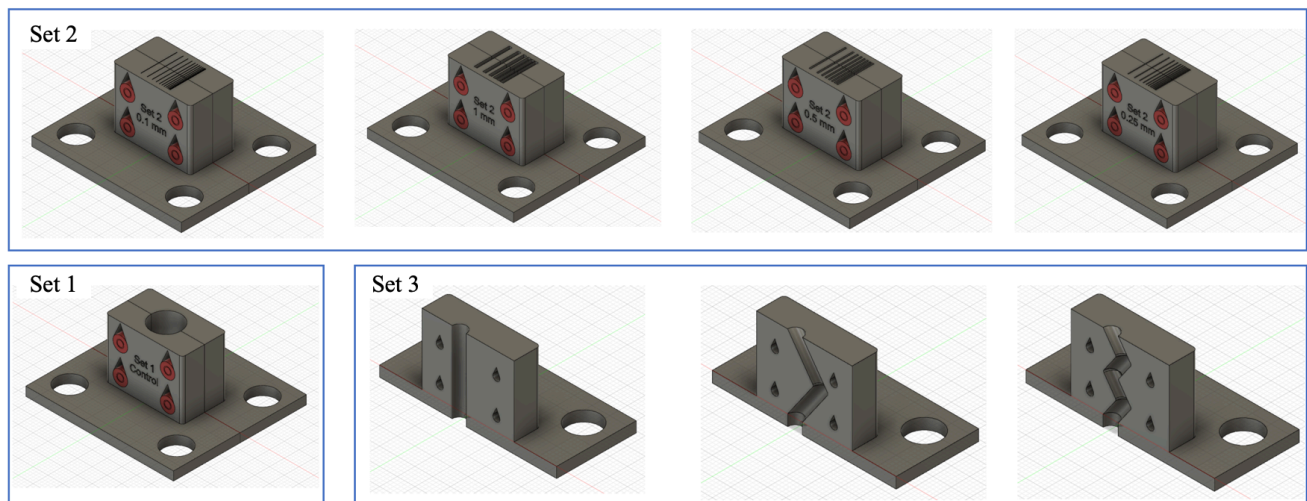


Figure 2: CAD drawings for all specimens.

3. Experimental

3.1. AM fabrication

AM fabrication of Ti6Al4V specimens was performed using the 3DSystems ProX 320 L-PBF system. A 245W laser power, and 82 micron hatch spacing were used with a 60 micron layer thickness for a 100% dense part. The specimens were oriented such that the channels were printed in the z direction, perpendicular to the build plate.

After fabrication, the samples were removed from the build plate using wire-EDM. Each half of the specimens were filed to ensure flat surfaces on mating faces. Tapping operations were performed on the bolt holes to ensure a secure fit between the 2 halves when bolted. No heat treatment was performed on the parts.

3.2. AFM experimental procedure

AFM was carried out using the AFM Vector machine by Extrude Hone. 2-way flow was used for this experiment. The media, commercially branded as EM 25103, which was the lowest viscosity media available, was chosen.

The two halves of each specimen were bolted together and the entire specimen was bolted to the fixture placed between the 2 cylinders of the AFM machine. Once the media was loaded and the upper cylinder was lowered into position, the AFM parameters of 1300 psi (~9 MPa) media pressure and 1500 inch³ (~24.6 liters) were set. One AFM cycle was defined as one upward cylinder motion followed by one downward cylinder motion. 5 AFM cycles were performed on the Set 2 (rectangular channels and thin walls) specimens and 15 AFM cycles were performed on the Set 1 (10 mm diameter through hole) and the Set 3 (4 mm diameter bends) specimens. Cycle times for each specimen were noted.

Following AFM, Set 2's thin walled channels contained excess media buildup, and were stripped of excess abrasive material that was left behind via using carrier media to connect to leftover media in the channels. The media's respective surface tension was utilized, and in doing so, removed a majority of the material from the inlets and outlets of the channels, but proved to be insufficient towards the center of the specimen. Following the preliminary cleaning, the specimens were subjected to multiple cycles of ultrasonic cleaning in a bath of distilled water, rinsing out the broken-up media; drying off with compressed air. This cleaning cycle was repeated until no more abrasive media were found to depart from the small slits of the channels.

3.3. Micro-CT scanning procedure & inspection methodology

Considering the dimensions and geometry of the specimens, micro Computed Tomography (CT) was used as the method for inspection. Micro-CT scans were obtained for as-built and post-AFM samples using the GE v|tome|x L300 multi-scale nano/micro-CT system available at the Centre for Quantitative Imaging (CQI) at The Pennsylvania State University. A voxel size of 12 microns was chosen to obtain a high resolution sufficient to extract surface roughness data while maintaining reasonable scanning times.

The micro-CT data was obtained as .vol files which were imported to ImageJ for processing and measurements. After converting the data from 32-bit to 8-bit for ease of handling and computation, the slices were cropped to retain the data only containing the sample. The 8-bit images were exported as .tiff files for further analysis.

AFM involves material removal and one of the objectives of this research was to study to change in dimension of the additively manufactured specimen features. Dimension analysis was performed in ImageJ for both as-built and post-AFM specimens using the line tool followed by the measure command. After importing the 8-bit tiff stacks into ImageJ, it was observed that the images had a gradual shift in the grayscale values at the boundaries of the specimen features. In order to obtain a clear distinction between the material

and air, thresholding was applied to ensure the specimen material was represented using white pixels (255 grayscale value) while the air was represented by black pixels (0 grayscale value). Rotation and re-slicing operations were performed to obtain the 2D-slice view corresponding to the cross-section of the internal channels. For the rectangular channels (Set 2), the dimensions under consideration were the slot width and breadth, whereas radius was measured for both halves of the cylindrical channels (Set 1 & Set 3). Measurements locations are illustrated in Figure 3. Measurements were taken at equal intervals along the channel length based on 2D-slice numbers. For the cylindrical channels, radial measurements were taken at 45, 90, and 135 degrees as illustrated in Figure 3(a). Prior, to taking measurements, appropriate scaling was performed to convert the pixel value to mm using the voxel size of 12 microns. The line tool was used to create straight lines using the angle guide and dimension values were obtained using the Measure command.

Roughness analysis using micro-CT data was performed to analyze the change in surface roughness values of these internal channels. A novel method was developed to measure linear surface roughness using micro-CT data using ImageJ and Wolfram’s Mathematica program. This is described in Figure 4. After thresholding in ImageJ, the 2D-images were re-sliced such that the resulting slice represented the surface of interest. These were obtained using a linear re-slice command for the rectangular channels (Set 1), and using a radial re-slice command for the cylindrical channels. Appropriate cropping, rotating, and combining operations were performed on the channels with bends to obtain a straight profile for the channel surfaces prior to using radial-re-slice. After obtaining the surface of interest, the raw surface profile data was obtained using the Plot Profile command in ImageJ. This command provided a plot of the average grayscale value corresponding to every pixel along the length of the image. In order to convert the average grayscale value to mm, the following expression was used:

$$height (mm) = (voxel\ size (mm/pixel) \times average\ gray\ value \times height (pixels))/255$$

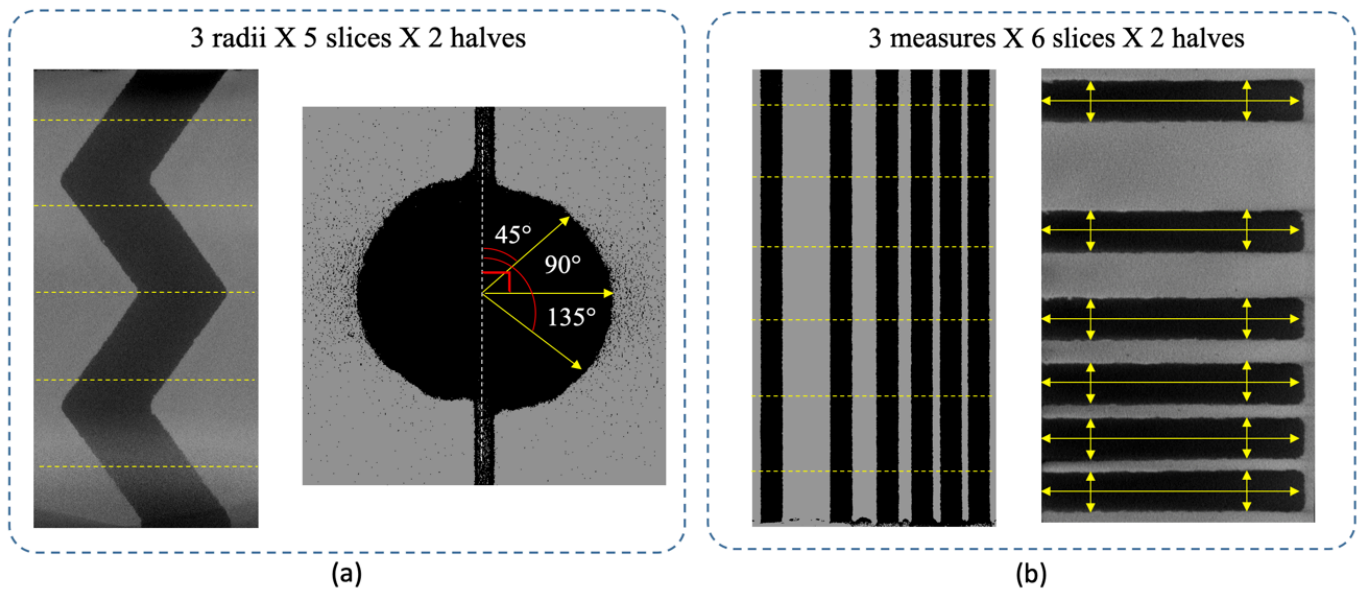


Figure 3: Illustrations of measurements taken for (a) radius of cylindrical specimens (b) slot width & breadth for rectangular channels

The resulting data was imported into Wolfram’s Mathematica and converted to a time-series data where the x-axis represented the length (in mm) and the y-axis represented the height (in mm). Before,

calculating the roughness values, the surface form was removed from the raw profile using the Lowpassfilter command. A cutoff wavelength of 2.5 mm based on the ASME B46.1 standard [22] was used to filter out frequencies higher than the provided cutoff. This was performed using a Fast Fourier Transform (FFT) in the Lowpassfilter command. The roughness profile was calculated by subtracting this result from the raw profile. Using the Mean, Max, and Min commands, the average roughness (Ra), maximum peak height (Rp), and minimum valley depth (Rv) values were obtained. The total profile height (Rt) was calculated by subtracting the Rv values from the Rp values. Roughness calculations were performed at three locations of every surface of each half for both as-built and post-AFM specimens.

In order to better visualize the areas affected by the process, in addition to surface texture change, the tiff stacks were imported into Avizo. Segmentation was performed on the stacks to extract the data corresponding to the material. The segmented data was converted to a surface using the Generate Surface tool within Avizo without any smoothing to retain surface detail. The resulting surface consisted of a large number of triangles which were reduced to about 1/10th of their original size and exported as STL files for ease of handling. This was used for both surface texture visualization and to create deviation maps. Geomagic Control X by 3D Systems was used to create the deviation maps. The STL meshes were imported into Control X as measured data and compared to the STEP files of the specimen using the 3D Compare tool.

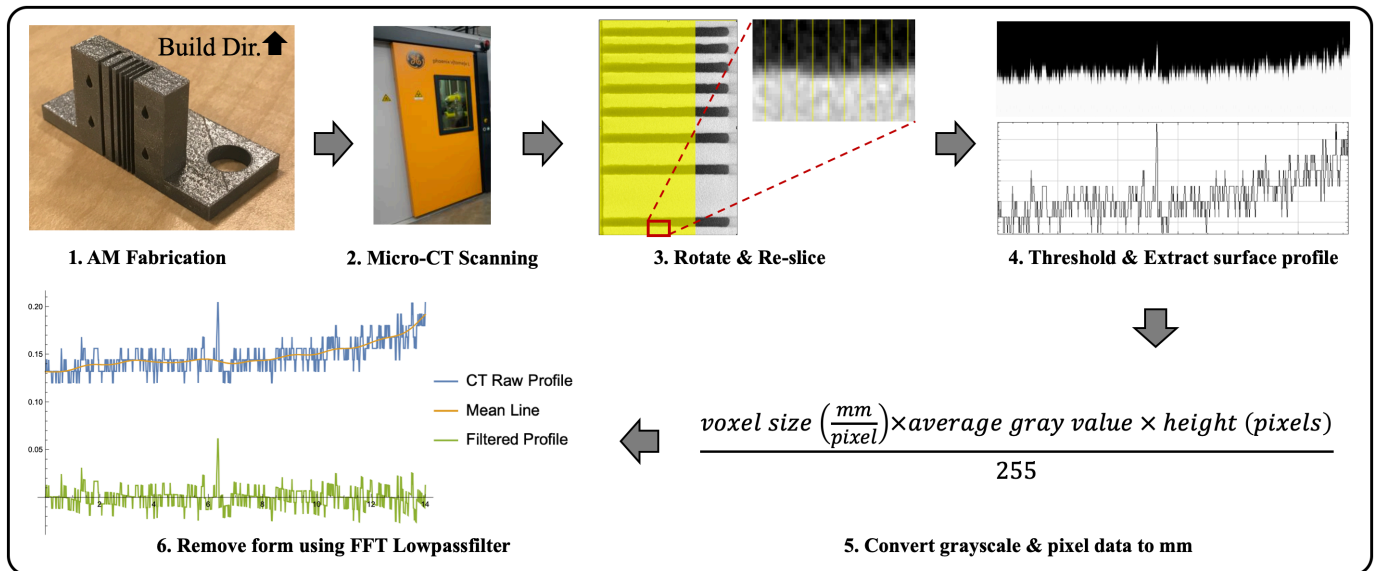


Figure 4: Illustration of the roughness using micro-CT methodology

4. Results & Discussion

The micro-CT scans showed that the as-built 0.1 mm slots were fabricated with insufficient space for media to flow through and thus no AFM was performed on it. Using the decided AFM parameters along with the choice of media resulted in approximately 6 hours of cycle time for the 0.25 mm slots, and therefore eliminated from this study. The remaining specimens were analyzed for cycle times, dimension, and surface roughness variations.

Most significant cycle time variations were recorded for the Set 2 1 mm and 0.5 mm specimens. The cycle times reduced with increasing number of cycles. For the 1 mm slots, the cycle time reduced from 69 seconds to

26 seconds, and for the 0.5 mm slots the cycle times reduced from 755 seconds to 172 seconds after 5 cycles, respectively. These were a result of increasing slot width with material being removed by the cutting action of the abrasive particles allowing more media to flow through it.

4.1. Surface roughness

Post-AFM surface roughness measurements were compared to as-built for each specimen. Figure 5 shows the change in surface roughness values before and after the AFM process for the Set 1 specimen. Average Ra value reduced by 40.67%, from 10.66 μm to 6.32 μm , and the average Rt value reduced by 47.45%, from 97.1 μm to 51.03 μm after 15 cycles. Another finding was the reduction in variation of surface roughness measured by a 64.2% and 69.68% reduction in standard deviation of the Ra and Rt values respectively. It can be concluded that for the 10 mm diameter through hole Set 1 specimen, there was a significant improvement of surface roughness in both smoothing (reduction in average Ra & Rt) as well as uniformity (reduction in standard deviations of Ra & Rt) after 15 cycles.

Each surface of each slot was analyzed for surface roughness in the Set 2 specimens. Ra values measured before and after AFM are presented in Figure 6. The average Ra value for 0.5 mm slots reduced in a range between 10.18% to 31.29%. There was also a reduction in standard deviation for all surfaces that ranged from 38.82% to 86.73%. The average Ra values reduced for all surfaces of the 1 mm slots ranging from 5.55% to 19.81%. However, surfaces 2, 3, 4, and 5 showed an increase in post-AFM Ra standard deviation by up to 3 times as the as-built Ra standard deviation. Ra standard deviation reductions of 8.72% to 50.1% was observed for all other surfaces. It can be concluded that after just 5 cycles, there was a significant improvement in surface roughness values in terms of both smoothing and uniformity of thin wall surfaces for 0.5 mm slots. However, for the larger 1 mm slots, there was reduction in Ra values observed, but certain surfaces with thinner walls showed an increased variability of the Ra value that suggested non-uniform surface roughness. Another observation was that the magnitude of reduction of Ra value was greater for the smaller 0.5 mm slots as compared to the larger 1 mm slots for the same number of cycles.

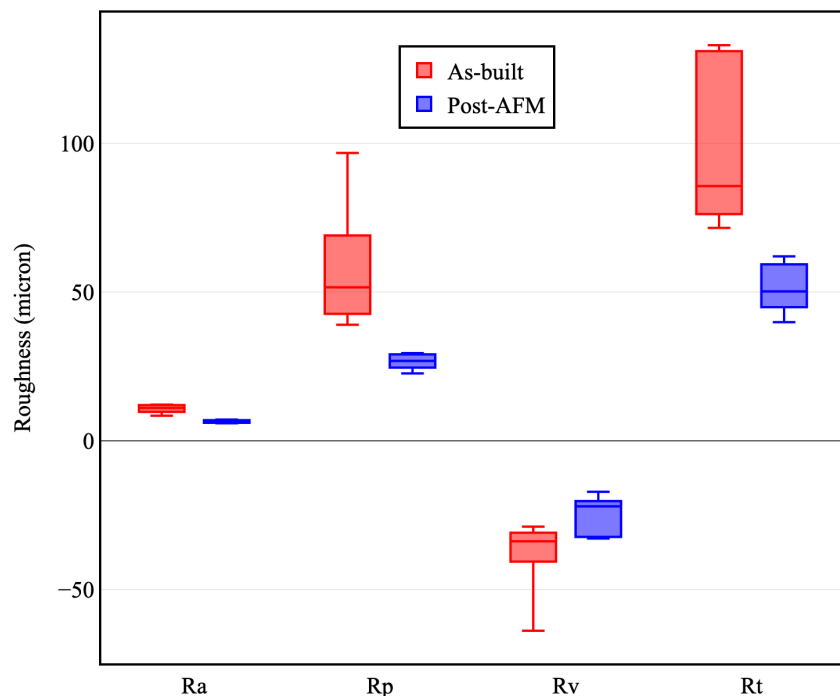


Figure 5: As-built v/s post-AFM comparison of Set 1 specimen

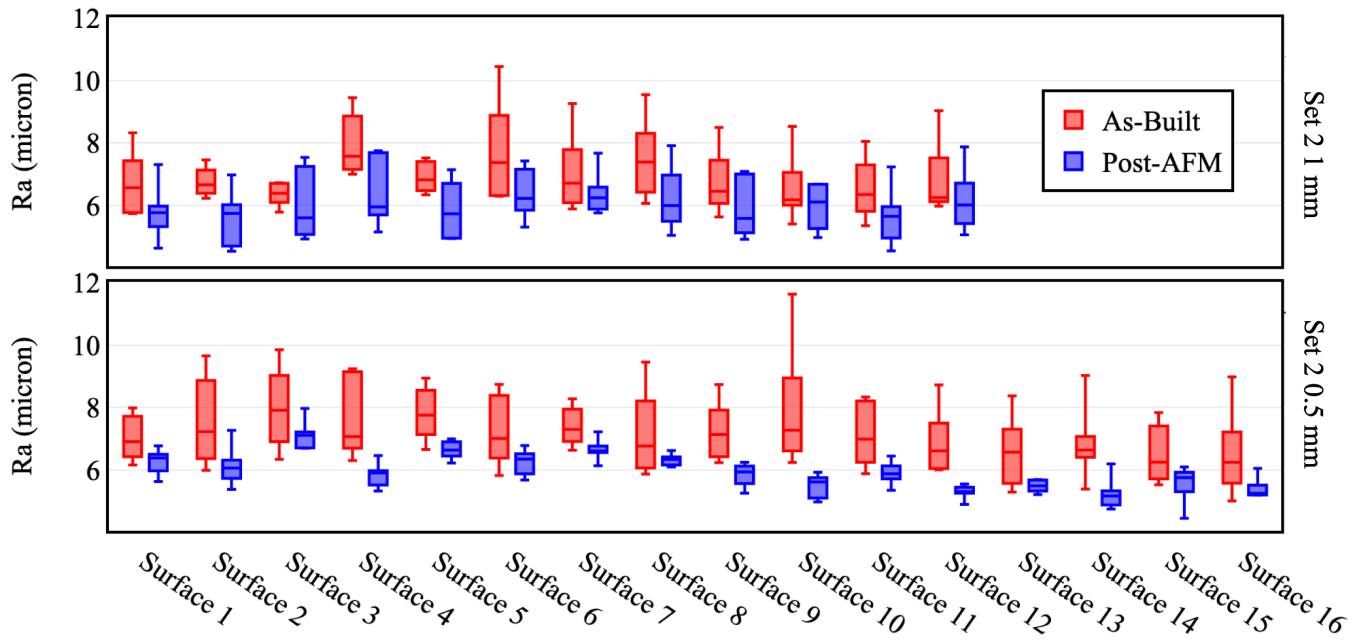


Figure 6: As-built v/s post-AFM comparison of Set 2 specimens

The Set 3 specimens results are presented in Figure 7. It showed similar trends as Set 1 with reduction in both average Ra values as well as reduction in standard deviation of the Ra values. The average Ra values reduced by 20.4%, 38.34%, and 38.46% for the control, 1 bend and 3 bend specimens, The standard deviation of the Ra values reduced by 58.74%, 43.09%, and 75.19% for the control, 1 bend, and 3 bend specimens.

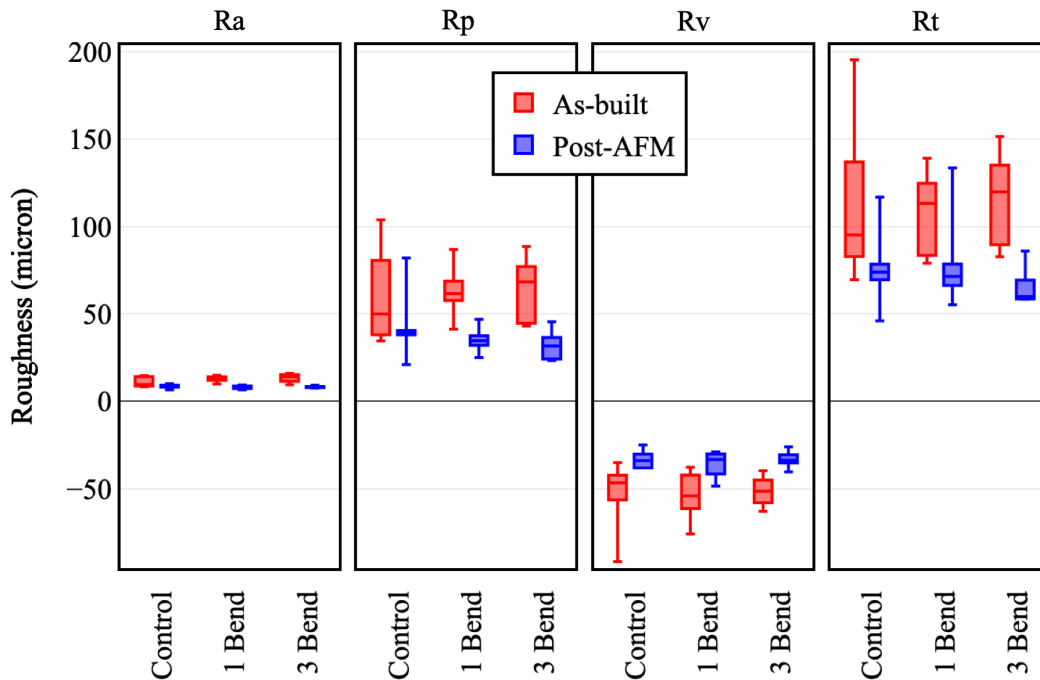


Figure 7: As-built v/s post-AFM comparison of Set 3 specimens

4.2. Dimensions

Dimension measurements were taken on the as-built and post-AFM micro-CT scans of each specimen. As per Figure 8 the radius of the Set 1 specimen remained largely unchanged. This was validated using a one-way ANOVA test which gave a p-value of 0.543, concluding that the means had larger variation within the conditions as compared to between the conditions. However, it was noted that there was a reduction in the standard deviation by 39.92% which was likely a result of peaks being washed down by the process causing a slight increase in radius at those locations.

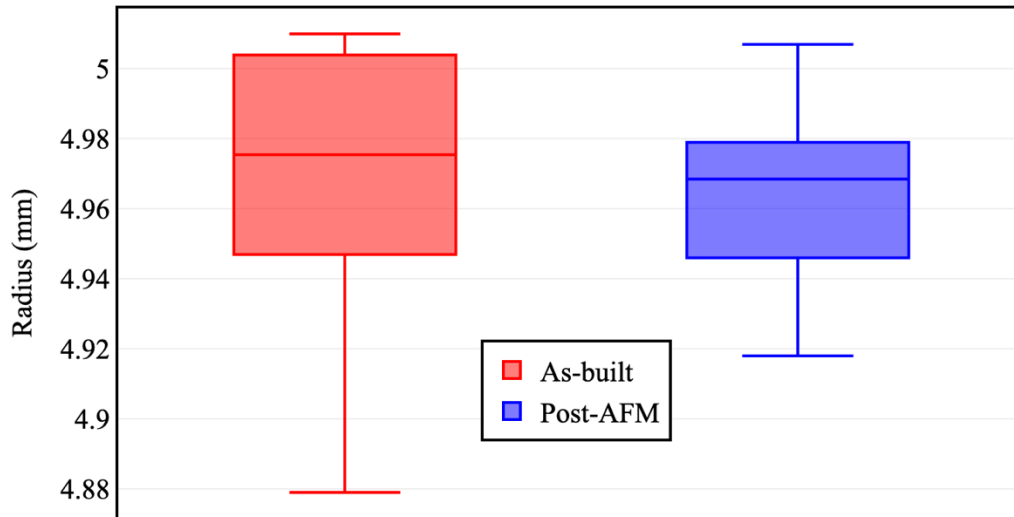


Figure 8: As-built v/s post-AFM radius comparison for Set 1 specimen

Dimensions in Set 2 underwent significant change. Figure 9 shows the first visual observation revealed deformation of three thin walls of 0.5 mm, 0.4 mm, and 0.3 mm within the 0.5 mm specimen. After removing the media, there seemed to be certain particles lodged into the channels. The micro-CT scan settings did not capture the region containing the largest deformation due to a shorter field of view. However, upon scanning a sample of the media revealed large abrasive grains (~2.63 mm) as well as traces of dense material having a CT signature similar to that of metals as shown in Figure 10. Such contaminants could be a part of previous workpieces that the media has been passed through causing chips to be incorporated into it, or could be a part of the current workpiece. Few of such contaminants having dimensions larger than the slot width, caused the thin walls to deform at the inlets under the media pressure.

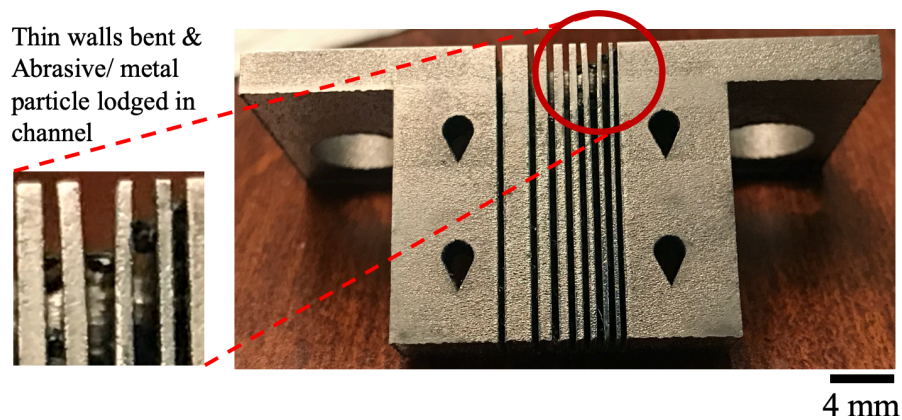


Figure 9: Image of the bent thin wall in the Set 2 0.5 mm specimen

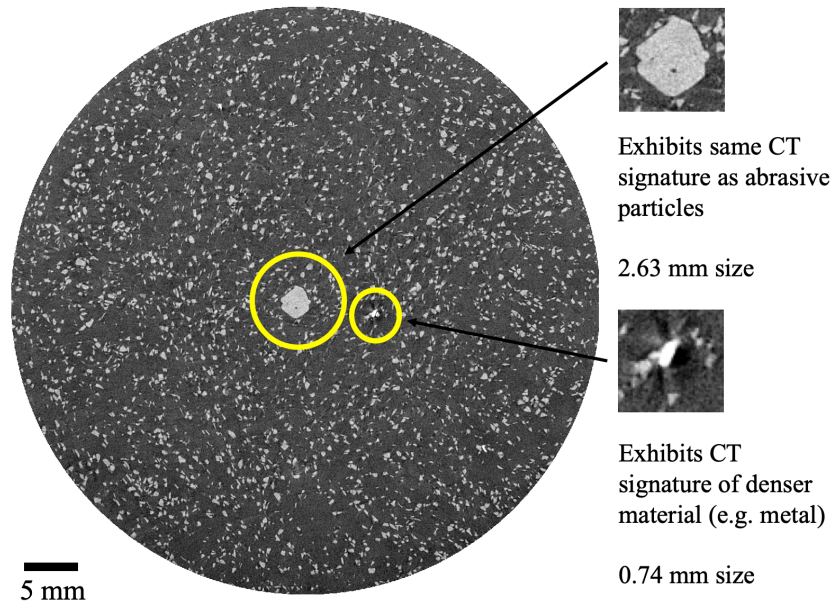


Figure 10: Micro-CT scan of the abrasive media

Overall, the slot width of every slot in the 0.5 mm specimen, other than Slot 1, increased. The largest deviation of 0.216 mm was observed in Slot 3. Slot 1 showed a reduction due to the thin wall bend.

For the 1 mm slot width sample, similar observations were made. The thinner 0.25 mm and 0.2 mm walls were deformed while the other walls were not. Slot 2 underwent the largest change of 5.85% in average slot width. The maximum deviation was 0.147 mm. Slot 1 showed reduction in average slot width due to deformation of the thin wall, whereas all other slots showed an increase in average slot width. Additionally, the standard deviation for slot width increased in the post AFM samples for all slots. This indicated an increase in the variability of dimension along the length of the rectangular channels. The results for the 0.5 mm and 1 mm samples are summarized in Figure 11.

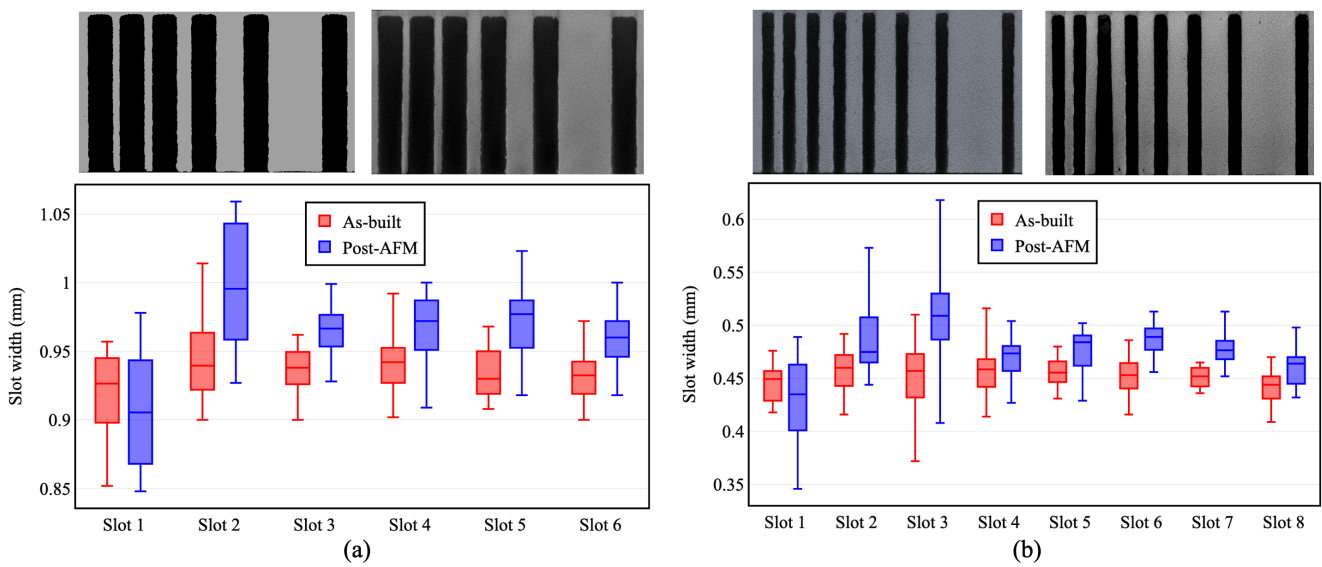


Figure 11: As-built v/s post-AFM slot width comparison for Set 2 specimens (a) 1 mm; (b) 0.5 mm

For the Set 3 specimens, about a 6% increase in the average value of the radius was observed for all 3 specimens after 15 cycles. The standard deviation for the Control and 3 Bend specimens increased by 3% and 37% respectively while it reduced by 13% for the 1 Bend specimen. The results are summarized in Figure 12. Thus, the variability in the radius along the length of the channel increased for the Control and 3 Bend specimens and reduced for the 1 Bend specimen after 15 cycles.

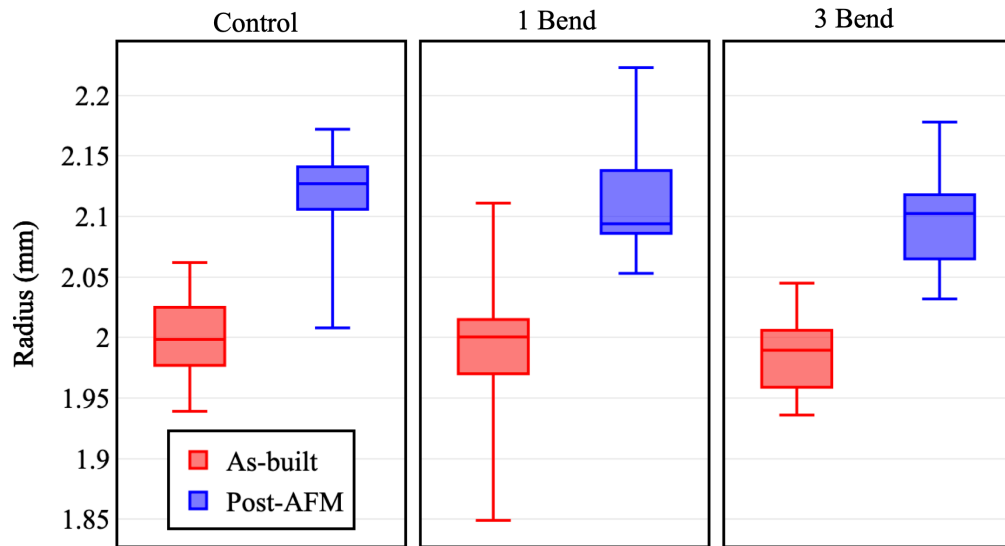


Figure 12: As-built v/s post-AFM comparison of radius for Set 3 specimens

In order to visualize the regions that were affected by the process, deviation maps were created using reconstructed CT data. Figure 13 shows the deviation maps of the as-built and post-AFM CT-reconstructions superimposed over the CAD STEP file. Shades of yellow, orange, and red represent the surfaces that extend above the CAD surface indicating the inherent surface roughness of the as-built workpiece. Deviation map of the post-AFM specimen shows blue areas that indicated the recessed surface caused as a result of the AFM process. The reconstructed models display the changes in surface texture caused due to the material removal action of the abrasive grain on the surfaces of the internal channels. Figure 14 clearly shows the markings created by the abrasive grains along the direction of flow of media inside the channel after 15 cycles.

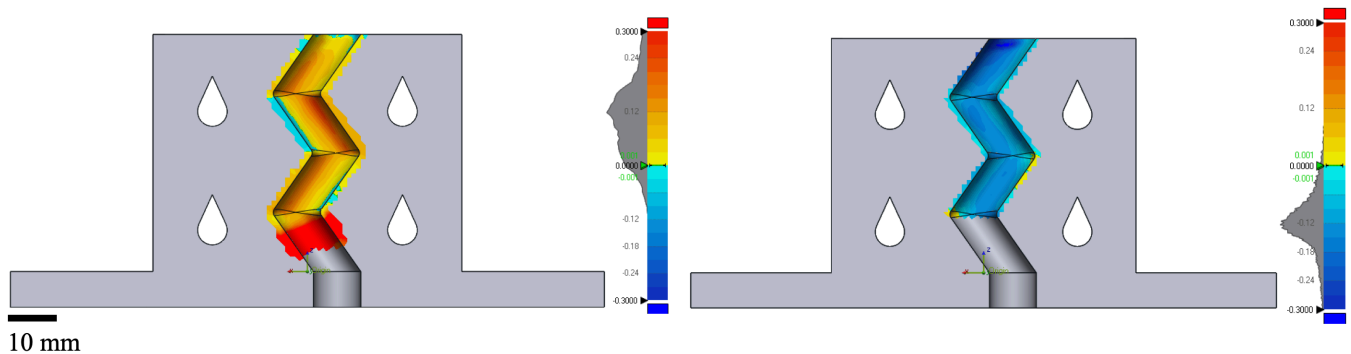


Figure 13: As-built (left) v/s post-AFM (right) comparison of deviation maps for Set 3 3 bend specimen

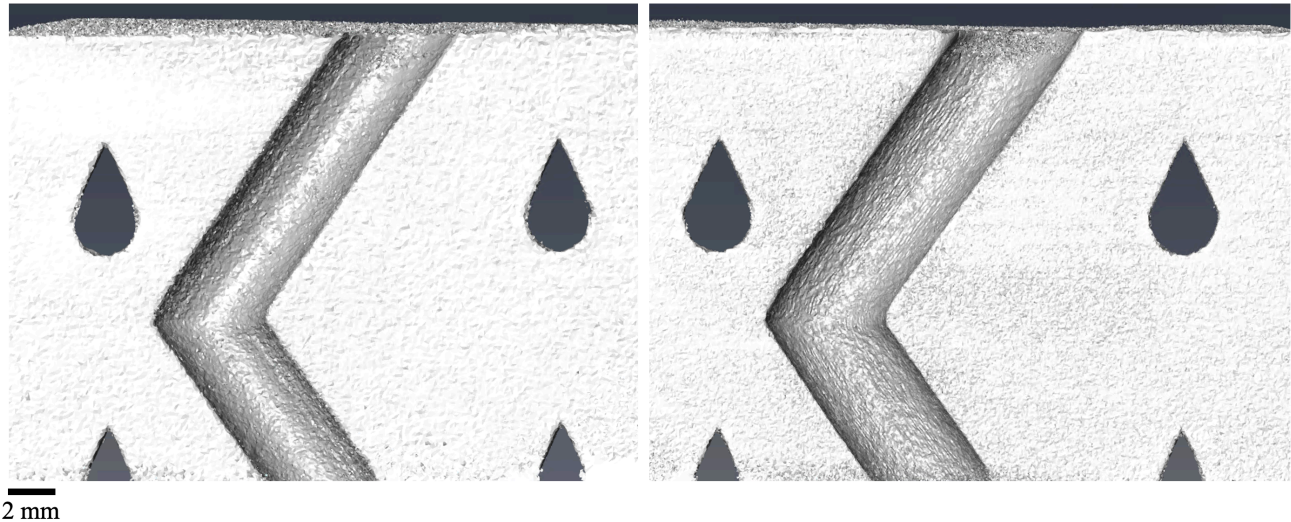


Figure 14: As-built (left) v/s post-AFM (right) CT reconstructions of the Set 3 1 Bend specimen

5. Conclusion

Abrasive flow machining is one of the few finishing and polishing methods that effectively enables post-processing of additively manufactured internal channels to improve surface roughness. 8 different specimens were manufactured using L-PBF to represent thin walls, through holes, and bends as internal channel geometries. The thin walled specimens were subjected to 5 AFM cycles while the through holes and bend specimens were subjected to 15 AFM cycles. Out of the initial 8 specimens, only 6 were machined since the specimens with 0.1 mm and 0.25 mm slots could not be machined due to improper fabrication and unreasonable AFM cycle time, respectively. Thus, media selection is an important aspect of the AFM process planning.

Micro-CT was used as a non-destructive method to evaluate changes in dimensions and surface roughness as a result of the AFM process. For the larger through hole specimen, there was a reduction in both average value and standard deviation of surface roughness while there was a reduction in variability of radius along the length of the channel. For the thin walls and rectangular channels, it was observed that walls thinner than 0.5 mm were deformed by the AFM media pressure. There was a reduction in surface roughness for all internal surfaces of the rectangular slots. However, it was noted that the resulting surfaces had varying values of surface roughness based on the respective as-built/initial surface roughness value. It can be concluded that for a specimen having multiple ports of entry, it is not certain that all internal channel surfaces will have uniform surface roughness values after the 5 AFM cycles. For the specimens with the bend(s) and the smaller diameter through hole it was observed that there was a reduction in surface roughness and an increase in radius after 15 AFM cycles. A reduction in standard deviation of Ra values was observed but the standard deviation of radius of the 3 bend and through hole specimen increased after the AFM process.

Overall, it can be concluded that internal channels having cross-sections of smaller dimensions (rectangular slot widths & 4 mm diameter cylindrical channels) showed increased variability in dimensions whereas the larger dimension specimen (10 mm diameter through hole) underwent no change in dimension while reducing variability along the length of the channel. It must be noted that all these conclusions are made for the specific media using which the experiments were performed. Future studies would incorporate a design of experiments with varying media while keeping the process parameters unchanged. More cycles

could also be performed on these channels to assess if the process is able to reach uniform, desirable surface roughness values and the variation in dimension observed in the process.

The AFM process resulted in the reduction of surface roughness of additively manufactured internal surfaces but caused deformation and dimensional changes. These variations are critical for the functionality of several potential applications that could benefit from the geometric complexity achieved using the L-PBF process. It is necessary to plan for these outcomes and create compensation models to incorporate them into the manufacturing process plan at the design phase itself.

References

- [1] “Heat Exchangers Market worth \$20.5 billion by 2024.” [Online]. Available: <https://www.marketsandmarkets.com/PressReleases/heat-exchanger.asp>. [Accessed: 23-Sep-2020].
- [2] “Contract Injection Molding Manufacturing in the US - Industry Data, Trends, Stats | IBISWorld.” [Online]. Available: <https://www.ibisworld.com/united-states/market-research-reports/contract-injection-molding-manufacturing-industry/>. [Accessed: 23-Sep-2020].
- [3] “AMPOWER Report on Metal Additive Manufacturing Market.” [Online]. Available: <https://additive-manufacturing-report.com/>. [Accessed: 23-Sep-2020].
- [4] B. Whip, L. Sheridan, and J. Gockel, “The effect of primary processing parameters on surface roughness in laser powder bed additive manufacturing,” *Int. J. Adv. Manuf. Technol.*, vol. 103, no. 9–12, pp. 4411–4422, Aug. 2019.
- [5] K. Mumtaz and N. Hopkinson, “Top surface and side roughness of Inconel 625 parts processed using selective laser melting,” *Rapid Prototyp. J.*, vol. 15, no. 2, pp. 96–103, Mar. 2009.
- [6] I. Koutiri, E. Pessard, P. Peyre, O. Amlou, and T. De Terris, “Influence of SLM process parameters on the surface finish, porosity rate and fatigue behavior of as-built Inconel 625 parts,” *J. Mater. Process. Technol.*, vol. 255, pp. 536–546, May 2018.
- [7] F. Caiazzo, V. Alfieri, M. V. Aliberti, and P. Argenio, “Influence of building parameters on surface aspect and roughness in additive manufactured metal parts,” *Key Eng. Mater.*, vol. 813, pp. 104–109, 2019.
- [8] A. C. Petare and N. K. Jain, “A critical review of past research and advances in abrasive flow finishing process,” *International Journal of Advanced Manufacturing Technology*, vol. 97, no. 1–4. Springer London, pp. 741–782, 01-Jul-2018.
- [9] V. K. Jain and S. G. Adsul, “Experimental investigations into abrasive flow machining (AFM),” *Int. J. Mach. Tools Manuf.*, vol. 40, no. 7, pp. 1003–1021, May 2000.
- [10] T. R. Loveless, R. E. Williams, and K. P. Rajurkar, “A study of the effects of abrasive-flow finishing on various machined surfaces,” *J. Mater. Process. Tech.*, vol. 47, no. 1–2, pp. 133–151, Dec. 1994.
- [11] W. Chih-Hua, K. Chun Wai, W. Stephen Yee Ming, and A. B. Adri Muhammad,

- “Numerical and experimental investigation of abrasive flow machining of branching channels,” *Int. J. Adv. Manuf. Technol.*, vol. 108, no. 9–10, pp. 2945–2966, Jun. 2020.
- [12] C. Bouland, V. Urlea, K. Beaubier, M. Samoilenko, and V. Brailovski, “Abrasive flow machining of laser powder bed-fused parts: Numerical modeling and experimental validation,” *J. Mater. Process. Technol.*, vol. 273, p. 116262, Nov. 2019.
- [13] S. Han, F. Salvatore, J. Rech, J. Bajolet, and J. Courbon, “Surface integrity in abrasive flow machining (AFM) of internal channels created by selective laser melting (SLM) in different building directions,” in *Procedia CIRP*, 2020, vol. 87, pp. 315–320.
- [14] S. Han, F. Salvatore, J. Rech, and J. Bajolet, “Abrasive flow machining (AFM) finishing of conformal cooling channels created by selective laser melting (SLM),” *Precis. Eng.*, vol. 64, pp. 20–33, Jul. 2020.
- [15] M. S. Duval-Chaneac, S. Han, C. Claudin, F. Salvatore, J. Bajolet, and J. Rech, “Experimental study on finishing of internal laser melting (SLM) surface with abrasive flow machining (AFM),” *Precis. Eng.*, vol. 54, pp. 1–6, Oct. 2018.
- [16] C. W. Kum, C. H. Wu, S. Wan, and C. W. Kang, “Prediction and compensation of material removal for abrasive flow machining of additively manufactured metal components,” *J. Mater. Process. Technol.*, vol. 282, p. 116704, Aug. 2020.
- [17] J. C. Snyder, C. K. Stimpson, K. A. Thole, and D. J. Mongillo, “Build Direction Effects on Microchannel Tolerance and Surface Roughness,” *J. Mech. Des. Trans. ASME*, vol. 137, no. 11, Nov. 2015.
- [18] A. Townsend, L. Pagani, L. Blunt, P. J. Scott, and X. Jiang, “Factors affecting the accuracy of areal surface texture data extraction from X-ray CT,” *CIRP Ann. - Manuf. Technol.*, vol. 66, no. 1, pp. 547–550, Jan. 2017.
- [19] G. Kerckhofs, G. Pyka, M. Moesen, S. Van Bael, J. Schrooten, and M. Wevers, “High-resolution microfocus X-ray computed tomography for 3d surface roughness measurements of additive manufactured porous materials,” *Adv. Eng. Mater.*, vol. 15, no. 3, pp. 153–158, Mar. 2013.
- [20] G. Pyka, G. Kerckhofs, I. Papantoniou, M. Speirs, J. Schrooten, and M. Wevers, “Surface Roughness and Morphology Customization of Additive Manufactured Open Porous Ti6Al4V Structures,” *Materials (Basel)*, vol. 6, no. 10, pp. 4737–4757, Oct. 2013.
- [21] S. Carmignato, V. Aloisi, F. Medeossi, F. Zanini, and E. Savio, “Influence of surface roughness on computed tomography dimensional measurements,” *CIRP Ann. - Manuf. Technol.*, vol. 66, no. 1, pp. 499–502, Jan. 2017.
- [22] American Society of Mechanical Engineers. and American Society of Mechanical Engineers. Standards Committee B46. Classification and Designation of Surface Qualities., *Surface texture : surface roughness, waviness, and lay.* .